

Vessel Centerline Extraction Using New Center of Gravity Equations

Hasan H. Khaleel, Rahmita O. K. Rahmat, DM. Zamrin, Ramlan Mahmud, and Norwati Mustapha

Abstract—The extraction and tracking of the vessels and their centerlines of coronary artery vessels in 2D and 3D angiograms has been vital part of many clinical analysis studies. This paper presents a new approach to extract the centerlines of vessels using novel center of gravity equations. The new equations depend on the intensity value as their main factor to track the vessels and by applying the center of gravity technique it can lead to centerline extraction. The new algorithm is called New Center of Gravity (NCOG). NCOG algorithm consists of four stages. First stage is angiogram partitioning using Recursive data structure technique. The second stage is to calculate the gray pixels in each partition and compare them with a threshold value (T). The third stage is center of gravity (COG) calculation. The fourth and last stage is connecting the final COG points by lines. The algorithm using the new COG equations were applied on a raw of clinical data and the results showed high robustness in extract the centerlines of vessels. We can conclude that our approach is robust, time saving, and helpful tool in surgery management and scientific researches.

Index Terms—Angiogram, coronary artery, vessel extraction, vessel centerline extraction, center of gravity.

I. INTRODUCTION

Coronary angiograms are performed to guide physicians in the medical diagnosis and treatment of cardiac patients. Important advances in coronary angiography have been brought about with the help of medical imaging techniques such as biplane angiography and digital subtraction angiography (DSA), according to Baim [4].

Hasan H. Khaleel is with Department of Multimedia, Faculty of Computer Science and Information Technology, Universiti Putra Malaysia, 43400, Serdang, Selangor, Malaysia (e-mail: hassan.upm@gmail.com).

Rahmita O. K. Rahmat is with Department of Multimedia, Faculty of Computer Science and Information Technology, Universiti Putra Malaysia, 43400, Serdang, Selangor, Malaysia (e-mail: rahmita@fsktm.upm.edu.my).

DM. Zamrin is with the Heart and Lung Centre, National University of Malaysia Medical Centre, PPUKM, 56000, Cheras, Kuala Lumpur, Malaysia (e-mail: drzamrin@gmail.com).

Ramlan Mahmud is with Department of Multimedia, Faculty of Computer Science and Information Technology, Universiti Putra Malaysia, 43400, Serdang, Selangor, Malaysia (e-mail: ramlan@fsktm.upm.edu.my).

Norwati Mustapha is with Department of Multimedia, Faculty of Computer Science and Information Technology, Universiti Putra Malaysia, 43400, Serdang, Selangor, Malaysia (e-mail: norwati@fsktm.upm.edu.my).

Blood vessel delineation on medical images forms an essential step in solving several practical applications such as diagnosis of the vessels (e.g., stenosis or malformations) and registration of patient images obtained at different times. Veins and arteries have many observable features, including diameter, color, tortuosity (relative curvature), and opacity (reflectivity). Artery-vein crossing and patterns of small vessels can also serve as diagnose indicators. An accurate delineation of the boundaries of blood vessels makes precise measurements of these features possible. These measurements may then be applied to a variety of tasks, including diagnosis, treatment evaluation, and clinical study, according to Baim [4]. The vessel extraction is a vital process in nowadays medical images. The extraction or tracking of blood vessels have been needed a lot in scientific researches, diseases diagnosing, and surgery planning. Therefore, the object detection plays an important role in many image processing problems such as Khalil *et al.* [9]. Examples from medical imaging are marker recognition and leukocyte tracking. In remote sensing, tasks like automatic target recognition and delineation of particular areas are essential object recognition tasks, [19].

There has been a considerable amount of work done on the enhancement and extraction of curvilinear structures from 2D medical images, most of which has focused on the extraction of a specific anatomical structure from a specific imaging modality—for example, cerebral blood vessels from magnetic resonance angiography (MRA) images [20] and bronchial trees from lung CT images [14]. From the clinical point of view, digital subtraction angiography (DSA), which subtracts X-ray images without contrast material from X-ray angiograms, is currently regarded as the most reliable and accurate method of vascular imaging. However, MRA [17] is seen as a potential alternative to DSA. CT angiography and conventional magnetic resonance imaging (MRI) can also be used for vascular imaging, [18].

Surgical and interventional radiology procedures often involve the visualization and quantification of vessels, bronchi, bowels, ducts, or nerves in two-dimensional (2-D) and three-dimensional (3-D) medical data. These and other anatomic objects are tubular, i.e., they have nearly circular cross sections, smoothly varying radii, and possibly follow

tortuous paths and branch. Clinical applications involving tubular anatomy in magnetic resonance angiogram (MRA), X-ray computed tomography (CT), and 3-D ultrasound data include shunt length specification, virtual colonoscopy flight-path control, embolization planning, stenosis detection, radiation therapy treatment planning, and MRA/digital subtraction angiogram registration for intraoperative guidance. Compared to edge identification which is generally performed using small-scale measures, centerline identification can be performed by integrating over a large extent of a tubular object and, therefore, may be less sensitive to image noise, [3].

Detection of objects can be performed by approaches such as the Hough Transform, (non-) linear filters, or by pattern recognition techniques such as neural networks or support vector machines, [19]. Object recognition can also be performed by detecting the object boundaries, e.g., by dynamic programming or snakes. Most of these methods give as a result the most likely central pixel of each detected object, either directly by means of a filter response or indirectly by means of the centroid of all points on the boundary contour. When the positions of the objects need to be known with sub-pixel precision, an accurate and robust estimate can be obtained by computing its center of gravity, [19].

In this paper, we are going to show the way of coronary artery extraction by extracting the centroid using new center of gravity equations. The Center of Gravity (CoG) is a popular technique in a variety of fields [1, 15, 12], due to its ability to simplify the data of an object. We first divide the image (angiogram) into four partitions using Recursive data structure technique. Afterwards we calculate the number of gray scale points for each partition. If the number was greater than or equal to a specific threshold value (T), then we apply recursive technique again for that partition, or else we calculate the COG point for the specific partition. The COG used to be calculated using conventional equations, in this paper we improve new equations to work with medical images. After getting the COG points for the whole angiogram, we connect those CoGs by lines. The output shape of lines will represent both the coronary artery tree plus the centerline of the vessel because we extracted the COG points of the vessels using our new equations. The results showed that using our new equations could give more accurate output comparing to the conventional one.

II. Methods

The proposed methodology of the CoG algorithm achieved success by introducing four main steps to extract the CoG points from the masked gray scale angiograms. The first step is to mask the plain angiogram images to extract only the coronary arteries in gray scale format. The second step is to recursively divide the image into four equal partitions. The

third step, and by the end of the recursive division process, is to calculate the number of points (NoP) for each partition. In the fourth step, the NoP for each partition is compared to a threshold value (T) that is set by the user. If $NoP \geq T$ in the current partition, then the partition is recursively divided or else a CoG point is calculated. The calculation of the CoG of the points is done using two new proposed mathematical equations. Finally, after the calculation of all the CoGs for the entire angiogram, they will be linked by lines. Linking the CoGs by lines is a process to construct the same original coronary artery tree but using only the centerlines. In other words, the CoGs will be located at the center of the arteries in the final partitions of the divided angiogram. Therefore, linking these CoGs together will visualize the coronary arteries again but only by the centerlines. Therefore, it is a good approach to extract the centerlines of coronary arteries. The following subsections of the proposed methodology give the details of the four main steps; however, a brief description regarding the use of CoG technique for real objects is presented first.

A. Center of Gravity in Real Objects

The definition of a Center of Gravity (CoG) is the source of power that provides moral or physical strength, freedom of action, or will to act, [16], thus, the center of gravity is usually seen as the source of strength. The **center of gravity (CoG)** of an object is the average location of its weight. In physics, the center of gravity of an object is a point at which the object's mass can be assumed, for many purposes, to be concentrated. For example, if you hang an object from a string, the object's center of gravity will be directly below the string. The path of an object in orbit depends only on its center of gravity. Most astronomical objects are radially symmetric, causing both the center of gravity and the center of mass to coincide at the center of the sphere.

The **center of gravity** or **CoG** of an aircraft is the point at which the entire weight of the aircraft is assumed to be concentrated and at which point the aircraft would balance if suspended there, [6]. The **center of gravity** of a collection of masses is the point where all the weight of the object can be considered to be concentrated. If (x_{cg}, y_{cg}) are the coordinates of the center of gravity of a collection of point masses m_1, m_2, \dots , etc, located at coordinates $(x_1, y_1), (x_2, y_2), \dots$, respectively, as it was reported by Armes [2]:

$$(m_1 + m_2 + \dots)gx_{cog} = m_1gx_1 + m_2gx_2 + \dots \quad (1)$$

$$(m_1 + m_2 + \dots)gy_{cog} = m_1gy_1 + m_2gy_2 + \dots \quad (2)$$

solving for the x -coordinate of the center of gravity:

$$X_{cog} = \frac{\sum_{i=1}^n m_i x_i}{\sum_{i=1}^n m_i} \quad (3)$$

similarly, the y-coordinate of the center of gravity is:

$$Y_{cog} = \frac{\sum_{i=1}^n m_i y_i}{\sum_{i=1}^n m_i} \quad (4)$$

For real objects, the center of gravity could be calculated using specific equations. Let's use the example of two kids on a see-saw. The see-saw by itself weighs 30lbs. Since the see-saw is a symmetrical object, the CoG of the empty see-saw will be exactly in the center of symmetry. So, to calculate CoG in this example:

- (1) Calculate the weight of the basic object.
- (2) Calculate the additional weights.
- (3) Choose a starting point.
- (4) Measure the distances.
- (5) Multiply each distance by the respective weight.
- (6) Add the weights of all the objects.
- (7) Divide the total moment by the total weight.

To find the CoG of a 2D object, use Eq. (5) to find the CoG along the x-axis and Eq. (6) to find the CoG along the y-axis, where W represents the weight. The point at which they intersect is the center of gravity.

$$X_{cog} = \frac{\sum_{i=1}^n (x_i * W_i)}{\sum_{i=1}^n W_i} \quad (5)$$

$$Y_{cog} = \frac{\sum_{i=1}^n (y_i * W_i)}{\sum_{i=1}^n W_i} \quad (6)$$

The definition for center of gravity of a general mass distribution is $(\int r dW / \int dW)$ where dW is the differential of weight, r is the position vector and the integrals are to be interpreted as Stieltjes integrals over the entire body. They can however be expressed as more conventional Riemann or Lebesgue volume integrals for distributions that admit a density function, [8].

B. Center of Gravity in Images

For the center of gravity in images, it has been used rarely especially in medical images since the equations above need to be improved so they can fit with images. Dealing with images is different from dealing with real objects. In [19], an algorithm was used to locate objects in gray scale images using the center of gravity measures. They have studied the behavior of the (weighted) center of gravity measure as a function of additive noise present in the gray value image. Furthermore, they analyzed the influence of applying a threshold to the gray value image (which determines the weighing scheme) for a possible bias and variance of the center of gravity measure. The decision whether to apply a threshold to the gray value image or not, is basically a choice between accuracy and precision [Van Assen *et al.* (2002)]. In

order to find the best estimate for the center of gravity in a gray level image, a threshold should in general be applied to (the local neighborhood in) the image before calculating a center of gravity measure. The variance equation in the work makes it possible to estimate the trade-off between accuracy and precision, in the presence of noise [19].

In medical images and especially angiograms, upon which our method was built, we designed new equations to solve the problem. Vessel extraction has been taken a wide space in the medical articles since long time ago. But in this paper we present a new method to extract the vessels by extracting the centroid. CoG could be calculated using few equations as we said before. In Eq. (5) and Eq. (6), W represented the weight of the real object. Meanwhile, the weight could be omitted in Eq. (7) and Eq. (8) below. The x-axis in Eq. (7) or y-axis in Eq. (8) represents the main factor in the equations to calculate the CoG.

$$X_{cog} = \frac{\sum_{i=1}^n x_i}{n} \quad (7)$$

$$Y_{cog} = \frac{\sum_{i=1}^n y_i}{n} \quad (8)$$

We tried to apply Eq. (7) and Eq. (8) in our work to calculate the CoG in angiograms. In a previous algorithm [10, 11], we could reconstruct the 3D coronary artery tree but we had limitation which was the 3D object was represented as points in the 3D space. This led us to think of a way to connect the points of the vessels in 2D which can lead to connect those clouds of points in 3D in the future. We have designed the algorithm in this paper to connect the points of CoGs in 2D. Since we are dealing with huge data of coronary artery pints; therefore, it needs to construct a new data structure algorithm to connect these data. Our way to solve this problem is to use CoG technique. Using the conventional equations could give us some results to calculate CoG; however, studying the algorithm that was presented by Van Assen *et al.* [19], could sparkle in our mind proposing the new equations. Our new equations (Eq. (9) and Eq. (10)) involve the intensity value to be the main factor of calculating CoG;

$$X_{cog} = \frac{\sum_{i=x_1}^{x_2} \sum_{j=y_1}^{y_2} (i * g(i, j))}{\sum_{i=x_1}^{x_2} \sum_{j=y_1}^{y_2} g(i, j)} \quad (9)$$

$$Y_{cog} = \frac{\sum_{i=x_1}^{x_2} \sum_{j=y_1}^{y_2} (j * g(i, j))}{\sum_{i=x_1}^{x_2} \sum_{j=y_1}^{y_2} g(i, j)} \quad (10)$$

where X_{cog} is the x-coordinate of a CoG point and Y_{cog} is the y-coordinate of the CoG. x_1 and x_2 are the limits of a partition in the x-axis, y_1 and y_2 are the limits of the partition in the y-axis, and g is the intensity value of pixels. The term

$\sum_{i=x_1}^{x_2} \sum_{j=y_1}^{y_2} (i * g(i, j))$ indicates two summations and two limits. The first summation $\sum_{i=x_1}^{x_2}$ shows the x-axis limits of a partition and the second $\sum_{j=y_1}^{y_2}$ shows the y-axis limits of the same partition under consideration. Then the term $(i * g(i, j))$, where i is the x-axis factor and $g(i, j)$ is the gray scale value for vessel inside that partition. If the gray scale value is zero, the background, then the output will be zero. Therefore, no CoG will exist in this case, which means we are tracking the vessels down in the angiogram and not going for the parts that have no vessels. Then the term $\sum_{i=x_1}^{x_2} \sum_{j=y_1}^{y_2} g(i, j)$ which gets the summation of all gray scale values in that partition. Same for the y-axis of CoG point (Y_{cog}), in the term $\sum_{i=x_1}^{x_2} \sum_{j=y_1}^{y_2} (j * g(i, j))$, the j is y-axis factor and $g(i, j)$ is the gray scale value for vessel inside that partition.

The results of the CoG calculations using the conventional equations on our masked angiogram data were inaccurate as will be shown later in the results and their discussions. The new Eq. (9) is to calculate x-coordinate of the CoG point and Eq. (10) is to obtain the y-coordinate, i.e., (x_{cog}, y_{cog}) . The new equations include the intensity value of a pixel to extract the CoGs. As mentioned earlier, the intensity value element in the new equations will track down the gray scale arteries until the end of the angiogram and then stop. If, say $g(i, j)$ is the intensity value for a pixel located in row 'i' and column 'j', with x_1 and x_2 being the limits of the x-axis in the partition, and y_1 and y_2 are the y-axis limits in the same partition, then $\sum_{i=x_1}^{x_2} \sum_{j=y_1}^{y_2} g(i, j)$ represents the summation of all intensity values in the entire partition. The proof of the correctness of Eq. (9) and Eq. (10) is by generalizing them from the conventional equations (Eq. (7) and Eq. (8)). The proof of the generality of the new equations (Eq. (9) and Eq. (10)) is shown as follows.

Theorem 1. *The new equations (Eq. (9) and Eq. (10)) are not general forms of the conventional equations (Eq. (7) and Eq. (8)).*

Proof. Let us assume that the value of $g(i, j) = 1$ for all rows 'i' and columns 'j' in the image. If we substitute this into the new equations, i.e., Eq. (9) and Eq. (10), we obtain the equations:

$$X_{cog} = \frac{\sum_{i=x_1}^{x_2} \sum_{j=y_1}^{y_2} (i * (1))}{\sum_{i=x_1}^{x_2} \sum_{j=y_1}^{y_2} (1)} \tag{11}$$

$$Y_{cog} = \frac{\sum_{i=x_1}^{x_2} \sum_{j=y_1}^{y_2} (j * (1))}{\sum_{i=x_1}^{x_2} \sum_{j=y_1}^{y_2} (1)} \tag{12}$$

Let us assume that the limits of a partition in the x-axis are between 1 and n, i.e., $x_1 = 1$ and $x_2 = n$. The numerator

$\sum_{i=x_1}^{x_2} \sum_{j=y_1}^{y_2} (i * (1))$ of Eq. (11) has two summations for both the x and y limits of a partition. After the substitution of the $x_1 = 1$ and $x_2 = n$ assumption and with a little algebra, the equations become as follows:

$$\begin{aligned} \sum_{i=1}^n \sum_{j=y_1}^{y_2} (i * (1)) &\Longrightarrow \sum_{j=y_1}^{y_2} \sum_{i=1}^n i \\ \Longrightarrow \sum_{i=1}^n i &\Longrightarrow \sum_{i=1}^n n \end{aligned}$$

As for the denominator of Eq. (11), with a little algebra it becomes as follows:

$$\sum_{i=x_1}^{x_2} \sum_{j=y_1}^{y_2} (1) \Longrightarrow \sum_{i=1}^n 1 = n$$

We rewrite Eq. (11) after substituting the newly obtained numerator and denominator above:

$$X_{cog} = \frac{\sum_{i=1}^n n}{n} \tag{13}$$

Let us say $n = x_i$, then Eq. (13) will become as follows:

$$X_{cog} = \frac{\sum_{i=1}^n x_i}{n} \tag{14}$$

We can conclude now that Eq. (14) is identical with Eq. (7), which means that the new Eq. (9) is a general form of the conventional Eq. (7). Since this violates our assumption of Theorem 2.1., therefore, our assumption is wrong and the new Eq. (9) is indeed a general form of the conventional Eq. (7).

The same applies to the Eq. (12) in Theorem 2.1., the substitution and algebra simplification are as follows:

Let us assume that the limits of a partition in the y-axis are between 1 and n, i.e., $y_1 = 1$ and $y_2 = n$. The numerator $\sum_{i=x_1}^{x_2} \sum_{j=y_1}^{y_2} (j * (1))$ of Eq. (12) has two summations for both x and y limits of a partition. After the substitution of the $y_1 = 1$ and $y_2 = n$ assumption and with a little algebra, it becomes such as the following:

$$\begin{aligned} \sum_{i=x_1}^{x_2} \sum_{j=1}^n (j * (1)) &\Longrightarrow \sum_{i=x_1}^{x_2} \sum_{j=1}^n j \\ \Longrightarrow \sum_{j=1}^n j &\Longrightarrow \sum_{j=1}^n n \end{aligned}$$

As for the denominator of Eq. (12), with a little algebra it becomes as follows:

$$\sum_{i=x_1}^{x_2} \sum_{j=y_1}^{y_2} (1) \Longrightarrow \sum_{j=1}^n 1 = n$$

We rewrite Eq. (12) after substituting the newly obtained numerator and denominator above:

$$Y_{cog} = \frac{\sum_{j=1}^n n}{n} \tag{15}$$

Let us say $n = y_j$, Eq. (15) will become as follows:

$$X_{cog} = \frac{\sum_{j=1}^n y_j}{n} \tag{16}$$

We can conclude now that Eq. (16) is identical with Eq. (8), which means that the new Eq. (10) is a general form of the conventional Eq. (8). Since this violates our assumption of Theorem 2.1., therefore, our assumption is wrong and the new Eq. (10) is indeed a general form of the conventional Eq. (8).

We expected the new equations to give more robust and better results than the conventional equations after proving by Theorem 2.1. that the new suggested equations are general forms of the conventional equations. The question that might be raised at this point could be why do we expect better results from the new mathematical equations? The answer to this question is because of the new element that was included in the new equations, which is the intensity value. The conventional equations involved calculating the CoG coordinates from the average of all the pixels inside a partition or subparts no matter where their locations are within that partition. However, the new equations would track down the gray scale arteries, taking advantage of the intensity element in the equations, and always calculate the exact coordinates of the centroids. The results regarding the efficient behaviour of the new equations over the conventional equations will be shown later in the results section. Three assumptions will be discussed later to prove the robustness of the new equations over the conventional equations.

Both of the new suggested mathematical equations are responsible for calculating the CoG of the gray scale arteries in the masked angiograms. The equations are to extract the x and y coordinates of the centroids. The importance of suggesting the new equations is to calculate more accurate CoGs than the conventional equations. The conventional equations averaged the pixel values in the rows and columns to calculate the x_{cog} and y_{cog} respectively. However, the suggested equations in this chapter included the intensity value, which we expect it to extract more accurate results, as will be shown later in the experiments, results and discussion section. Therefore, the new equations will be used to calculate the CoGs for the work of this paper upon proving their correctness in Theorem 2.1. before and after the three assumptions that will be discussed later. The creation of the new equations helped to achieve the advantages of calculation of CoGs at the exact centers of the gray scale arteries and the calculation of the CoGs in an artery will continue until the end of the artery and will stop once the artery has disappeared from the angiogram. Fig. 1 illustrates a synthetic vessel with the calculated CoGs located at the center of the artery.

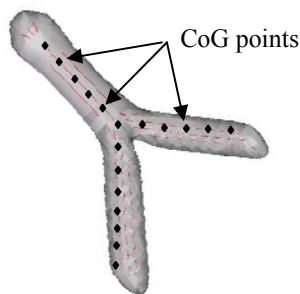


Fig. 1. Synthetic vessels with CoGs located at the center.

C. NCoG Algorithm

In this step of the methods, we present the whole flowchart of our new method to extract the arteries centerlines, as shown in Fig. 2. The method involves coronary artery centroid extraction using CoG technique. The steps of the method are as follows:

- (1) Mask the input plain angiogram,
- (2) Recursive division of the masked angiogram,
- (3) For each partition, find the Number of Points (NoP),
- (4) If $(\text{NoP} \geq T)$ - T is a threshold value – repeat steps 2 and 3, else go to step 5,
- (5) Calculate CoG point of the partition or subpart,
- (6) Once steps 2, 3, 4, and 5 are done for all angiogram's partitions and subparts, the calculated CoGs will be linked by lines according to Nearest Neighbor (NN) technique. Finally, the linked CoGs are displayed. The display stage is to visualize the extracted CoGs as one complete coronary artery tree.

D. NCoG Algorithm

In this step of the methods, we present the whole flowchart of our new method to extract the arteries centerlines, as shown in Fig. 2. The method involves coronary artery centroid extraction using CoG technique. The steps of the method are as follows:

- (1) Mask the input plain angiogram,
- (2) Recursive division of the masked angiogram,
- (3) For each partition, find the Number of Points (NoP),
- (4) If $(\text{NoP} \geq T)$ - T is a threshold value – repeat steps 2 and 3, else go to step 5,
- (5) Calculate CoG point of the partition or subpart,
- (6) Once steps 2, 3, 4, and 5 are done for all angiogram's partitions and subparts, the calculated CoGs will be linked by lines according to Nearest Neighbor (NN) technique. Finally, the linked CoGs are displayed. The display stage is to visualize the extracted CoGs as one complete coronary artery tree.

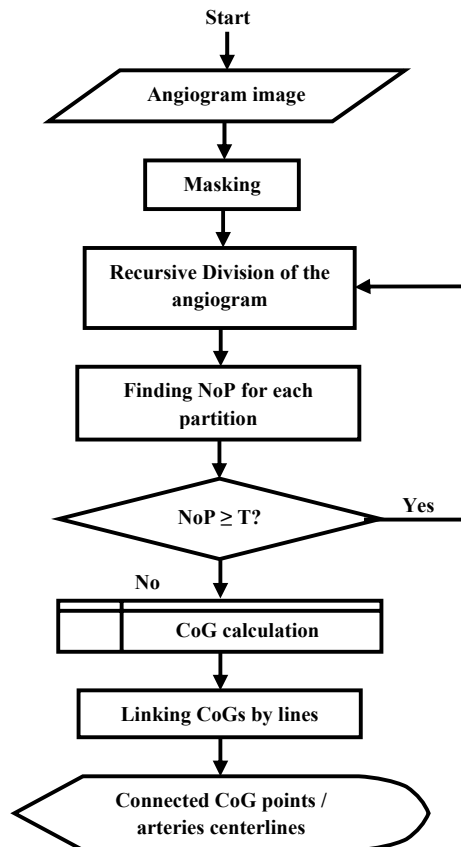


Fig. 2. The flowchart of the CoG algorithm.

Masking

Image processing has many important techniques and operations, and masking is one of these processes. The masking is a thresholding process that can isolate some features (the foreground) and remove others (the background) in order to highlight some objects from the whole image. For example, masking an image to include only pixels with values ≥ 100 and remove others. Therefore, the masking can be done generally by isolating some features which are below, equal, or above a specified pixel value. As it was explained by Luft *et al.* [13], the masking process isolates the boundaries of objects under consideration and slightly darkens the background to make the objects lighter. Since the masking process can be done manually by detecting objects in an image and isolate them; therefore, masking can be a semi-automatic operation. Medical images, as in other types of images, contain planes overlying other planes. The overlying planes belong to the foreground and others belong to the background.

The masking process firstly segmentizes all planes in an image according to a specific pixel value after determining that pixel value. Next, the segmented overlying planes will be extracted to a separate image to create what is called a *Binary Mask* with a “1” pixel value for the foreground and a “0” value for the background. Finally, the Binary Mask will be

combined with the original image to highlight the pixels with values higher than the specified pixel value in the masked image.

The specified pixel value in this paper of vessel extraction was “80”, i.e., all pixels with values higher than or equal “80” are saved in the masked image and the rest are zeroed-out (background). The value “80” is chosen after trying few values by experiment and this value worked well for all our angiograms. Thus, this value (80) can give good masking results without noise (noise refers to any background’s detection). The artery extraction in the gray scale format from the original image will be completed accurately because the Binary Mask will always determine which part of the image is required and which pixels to eliminate. Therefore, our extraction algorithm will first extract the binary coronary artery tree image and use it as a *Binary Mask* with the original angiogram image. The masking stage in this paper is important because we need to highlight only the coronary arteries from the plain angiogram and calculate the CoGs for them. However, the masking process is important for the 3D reconstruction algorithms recently where the idea of using the intensity values of pixels as the z-dimension in R^3 , [10, 11]. Fig. 3 illustrates the masking process in angiograms.

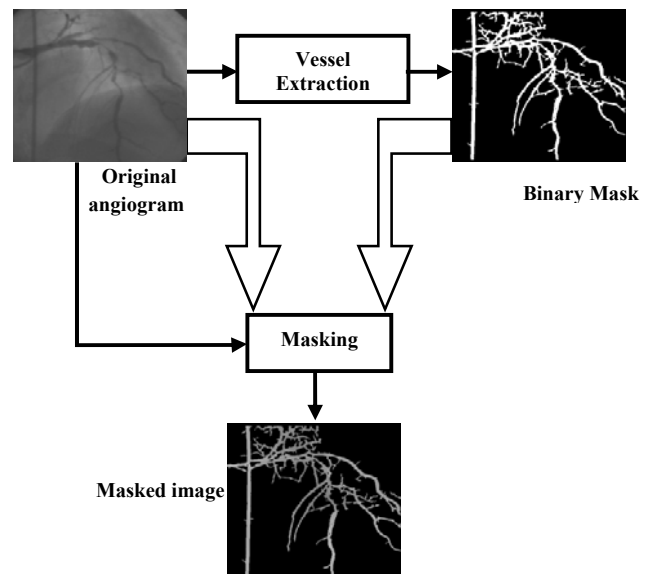


Fig. 3. Masking process in angiograms.

Recursive Division

In this section we will discuss the first stage of our algorithm in NCoG which is angiogram dividing. Since when we deal with medical images especially angiograms, we are dealing with huge amount of information. So, for the coronary artery angiograms there are thousands of points and dealing with them all at the same time would not be proper or could

give wrong results. In our algorithm we tried to use data structure conventional algorithms with our coronary artery trees but it did not fit to the acceptable level.

We thought of dividing the angiogram first into small partitions and deal with them separately then we gather the whole information for all partitions to get the total result for the whole coronary artery tree angiogram. In this paper, we used for the division the Recursive data structure technique. The divide approach is an iterative logical partitioning of a computation into isolated subparts, which can then be individually optimized part by part. The strategy is recursive, in that optimization of a subpart may itself involve further dividing and conquering. The overall optimized critical path is the maximum critical path among all parts [7].

The purpose of dividing is to break a difficult problem into more manageable parts. Our divide step both identifies and isolates subparts. As a result, the overall critical path lies within only one of the parts, and independent focused optimization of each computation subpart in accordance with its topological structure is enabled. An important ramification is that this enables the use of techniques which, while not applicable to the entire computation, can be applied to individual subparts [7]. Recursively defined data structures are essential constructs in programming languages. Intuitively, a data structure is recursively defined if it is partially composed of smaller or simpler instances of the same structure. Examples include lists, stacks, counters, trees, records and queues. To verify programs containing recursively defined data structures we must be able to reason about these data structures. Decision procedures for several data structures exist. However, in program verification decision procedures for a single theory are usually not applicable as programming languages often involve multiple data domains, resulting in verification conditions that span multiple theories. Common examples of such "mixed" constraints are combinations of data structures with integer constraints on the size of those structures [21].

In this paper we will divide the angiogram first into four equal parts. Then each part out of the four will be divided into four smaller parts. And we continue doing this to each and every partition until a stopping condition will be fulfilled. Our stopping condition in this paper will be depending on the number of points (intensity values) inside the partition itself. If the NoP inside a specific partition was larger than or equal to a threshold value we can set it (T) then divide again into four partitions or else calculate CoG of that partition. Fig. 4 shows the technique of division.

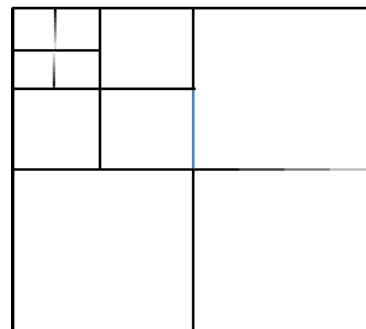


Fig. 4. Recursive division technique in images.

Finding NoP

In this step we are going to calculate the number of gray scale values (vessels) inside each partition. According to our equations, the limits of each partition would be ($i = x1$ to $x2$) for the x-axis and ($j = y1$ to $y2$) for the y-axis. So, we calculate the number of gray points inside these limits for each partition coming out from division step and that number will decide the next step for that specific partition. In the beginning of our algorithm we define a threshold value (T: a specific number) and this T will be the stopping condition of division. With each division process, we will compare the number of gray scale points inside each partition with T, so if NoP was larger or equal to T, we divide again or else we go for the next step which is calculating GoG. This step considers new approach to find the centroid of the vessels by calculating the CoG and it will be repeated for the whole angiogram.

CoG Calculation

Previous works, as in [19], has defined the CoG equation in different shapes. It has been always depending on the axes (x and y) as the main factor affecting the output. It used to calculate CoG by taking the mean of the object's points using Eq. (7) and Eq. (8) above. As it is clear, the equations' parameters play the main role in the output's robustness and affect it directly. Since our work depends totally on the vessels (objects) in our angiograms, we came out with the idea to derive new equations involve the gray scale value as one of the affecting parameters. The new equations that we derived (Eq. (9) and Eq. (10)) came out from Eq. (7) and Eq. (8) indicated above in this paper. As we explained previously that we involved the gray scale as the main affecting factor in our new equations because our input angiogram have black background and only gray scale vessels (objects) need to be tracked down. We tested the conventional equations and our new equations and the results are indicated in the experimental results section.

In this case, we are saving time, so instead of dividing the whole image and calculating CoG randomly, we will be specifying a condition here, which is there should be a gray

scale value (vessel) in that part to calculate CoG point for it. And this way will track the vessels down and calculate the centroid of them by getting CoG points. Fig. 5 indicates the CoG points in the middle of the vessel. We went through test the new equations and we came out with three assumptions showing the robustness of the new equations plus output enhancement over the conventional equations. The assumptions will be discussed in the discussion section after showing the results.

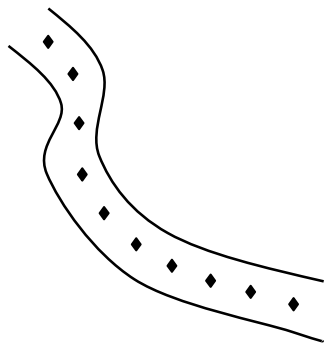


Fig. 5. A Synthetic vessel with its extracted CoGs located in the center.

Linking CoG Points by Lines

This is the last step of our approach when we attempt to link (connect) the extracted CoG points, which we extracted from previous step in section 2.3.4, by lines. The reasons from this connection are:

- (1) In order to give the CoG points the shape of the coronary artery tree that was used for CoG extraction,
- (2) Connecting those points will show the exact centroid of the vessels because the extracted CoG point was located exactly in the center of the vessel as in Fig. 6.

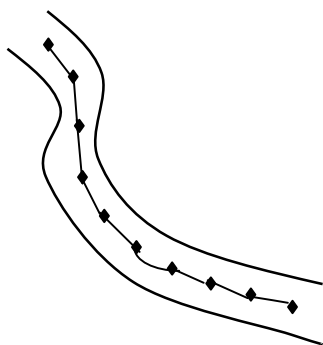


Fig. 6. A synthetic vessel with its extracted CoGs located in the center and linked by lines.

According to many papers and books about CoG technique, we found out that the center of gravity is the same as the center of mass. The key point is that the force of gravity on the object as a whole acts at the center of gravity. In order to determine the center of gravity for the patient-wheelchair

system, a balance platform was constructed in a manner similar to du Bois-Reymond [5]. This point – CoG – would be in the middle of an object and usually represents the mean of its surrounding points. This idea of CoG could be the same in images and objects included in them.

In this paper, we used the Nearest Neighbor (NN) technique to connect the CoG points by lines. This technique is going to check the surrounding points and grab the nearest one (Neighbor) and connect with it. Since the CoG points in our work will lie in the middle of the vessel and as in Fig. 5, then each point – except the two ending points – will have two neighbors, one above and the other below. So, each point will connect by lines with both neighbors, like in Fig. 6, and as a result will give a shape of connected lines or vessels. Since CoG points lie in the middle of the vessels, as we mentioned before, then the connected lines will represent the centroid of the vessels. By this way we could achieve two goals:

- (1) Extracting the vessel centroid,
- (2) Making our program more knowledgeable wise which point is connected or neighbor to which one in our coronary artery tree vessels.

In the past, plenty of researchers spent a lot of effort and time to extract the centroids (centerlines) of vessel using different complicated approaches. However, we present in this paper a simple yet robust approach to extract the centroids of vessels in angiograms using new proposed center of gravity equations. In the next section of experiments and results, we will show and prove the correctness of our new equations over the conventional.

III. EXPERIMENTAL RESULTS

The experiments are conducted by calling the results from the conventional Eq. (7) and Eq. (8) by *Algorithm-1*. However, the results from the new equations (Eq. (9) and Eq. (10)) were included under the name *Algorithm-2*. Therefore, *Algorithm-1* and *Algorithm-2* are applied on a row of 100 angiograms and their results are compared according to three assumptions will be discussed in the discussion section later on. The angiograms that are used in the experiments are collected clinically (real data). A database of 100 angiograms is built from around 10 patients. The size of angiograms is in the range of 512×512 resolution pixels. Both *Algorithm-1* and *Algorithm-2* are applied on the raw of angiograms and the results are shown in Fig. 7.

Fig. 7 shows few samples of our angiograms after applying *Algorithm-1* and *Algorithm-2*. We can notice some false alarms (errors) in the results of *Algorithm-1* while there is none of these false alarms in the results of *Algorithm-2*. It proves that the proposed equations can give more accurate results. Fig. 8 shows the same results from Fig. 7 but after taking out the vessels and leaving the linked centroids

standing alone from both algorithms (1 and 2). In this figure, we can notice the false alarms clearer than before after removing the vessels. Once more, Fig. 8 shows that the new equations can give better results than the conventional equations.

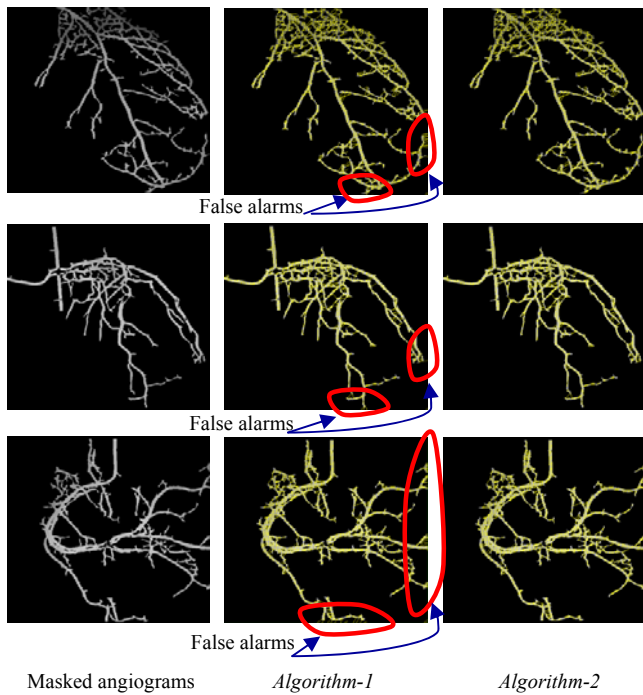


Fig. 7. The results of applying *Algorithm-1* and *Algorithm-2* on samples of angiograms.

To know the reason of the false alarms in the results of *Algorithm-1*, it is important to analyze the results of both algorithms and study them closely. We extracted the coordinates of the CoG points (X(cog) and Y(cog)) for both algorithms and we studied them closely. We found out that in *Algorithm-1*, the calculation of CoGs keeps generating these points till the end of the limits of the angiograms and that is because Eq. (7) and Eq. (8) depend totally on the image's coordinates only. Therefore, it will keep producing CoGs till the end of the image and subsequently can cause some false alarms in the connection part of CoG points. However, in *Algorithm-2* and since the new equations use the gray scale value as the main factor in CoG calculation; therefore, the algorithm keeps generating CoGs as long as there is a vessel (gray scale value). Thus, *Algorithm-1* will track down the vessel and terminate the calculations of CoGs when the vessel is finished even before the end of the angiogram. This fact is clearly noticeable in the values of coordinates of CoGs those were extracted from both algorithms. We can see zero coordinate values for the CoGs that are calculated at the end of angiograms when *Algorithm-2* is used. Therefore, no false alarms can be noticed in the results of *Algorithm-2*. On the other side, we can still see non-zero coordinate values for the

CoGs those are calculated at the end of angiograms when *Algorithm-1* is used. Table 1 and Table 2 show the coordinates of CoGs after applying both algorithms. Those coordinates are extracted from the calculations at the end of an angiogram.

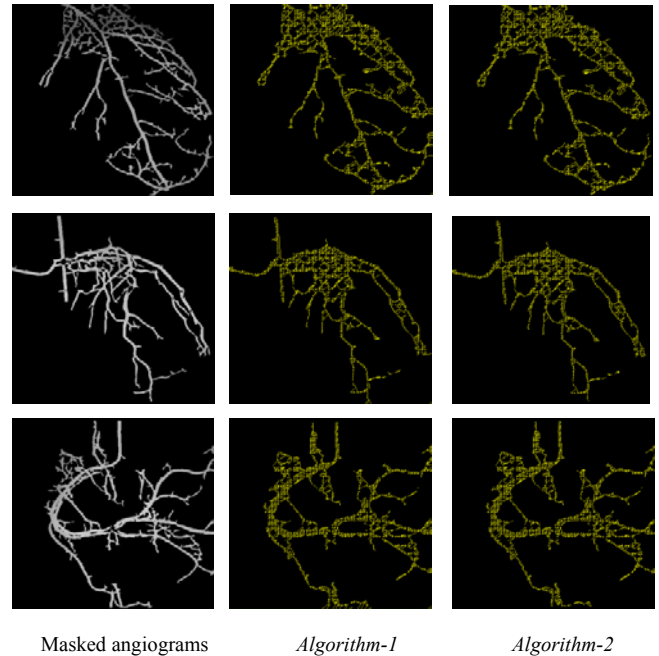


Fig. 8. Same results as Fig. 7 but with the linked centroids only.

TABLE I
COORDINATES OF COGS USING ALGORITHM-1

No. of partition	X(cog)	Y(cog)
3759	438	481
3760	443	483
3761	437	485
3762	441	485
3763	437	488
3764	441	488
3765	445	485
3766	448	486
3767	445	487
3768	448	487
3769	0	0
3770	0	0
3771	0	0
3772	0	0

TABLE II
COORDINATES OF COGS USING ALGORITHM-2.

No. of partition	X(cog)	Y(cog)
3759	437	485
3760	441	485
3761	437	488
3762	441	488
3763	445	485
3764	449	485
3765	445	487
3766	449	488
3767	428	506
3768	450	495
3769	439	506
3770	448	504
3771	439	506
3772	448	504

The results in Table 1 and Table 2 are just samples were taken from the end of the angiogram after applying both algorithms. We can notice from both tables above that there is 3772 CoG points are calculated in this angiogram, depends on the T that was chosen. The results in Table 1 show non-zero coordinate values until the end of the angiogram (X(cog) and Y(cog)), which causes false alarms. However, Table 2 results show zero coordinate values at the end of the angiogram because *Algorithm-2* keeps tracking vessels till their end only; therefore, there will be no more CoG points after this. This is first assumption of being the proposed equations better than the conventional equations.

In the meanwhile, we noticed that if *Algorithm-1* runs more than one time on the same angiogram, the results of X(cog) and Y(cog) will be changed. This was tested in 10 angiograms and the results of coordinates in 50% of them (5 angiograms) were changed. However, results stay always the same when *Algorithm-2* runs (new equations used). This fact was discovered by calculating the summation of errors in both CoGs coordinates and like the following:

$$\sum_{i=1}^n \Delta X(i) = (x(2) - x(1)) + (x(3) - x(2)) + \dots + (x(n) - x(n - 1)) \tag{17}$$

$$\sum_{i=1}^n \Delta Y(i) = (y(2) - y(1)) + (y(3) - y(2)) + \dots + (y(n) - y(n - 1)) \tag{18}$$

where **n** is the number of CoG points that are calculated in an angiogram through the entire process. Table 3 shows the fact of coordinates values changing upon running both algorithms two times on the same 10 angiograms. The algorithms run with T=30. The changed results were highlighted and marked with star (*) symbol.

TABLE III
T = 30. A) FIRST ITERATION OF RUNNING *ALGORITHM-1* ON 10 ANGIOGRAMS. B) SECOND ITERATION OF RUNNING *ALGORITHM-1* ON THE SAME 10 ANGIOGRAMS. C) FIRST ITERATION OF RUNNING *ALGORITHM-2* ON THE SAME 10 ANGIOGRAMS. D) SECOND ITERATION OF RUNNING *ALGORITHM-2* ON THE SAME 10 ANGIOGRAMS.

No. of image	No. of the calculated COG	ΣΔX	ΣΔY
1	3770	21987	22491
2	2821	18498*	18713*
3	3548	22861*	22965*
4	3554	22485	22989
5	4864	31703	32206
6	3427	21631*	21826*
7	4693	29590*	29618*
8	4361	28265	28767
9	3681	23935	24428
10	1815	11639*	11720*

(A)

No. of image	No. of the calculated COG	ΣΔX	ΣΔY
1	3770	21987	22491
2	2821	18872*	19378*
3	3548	23291*	23795*
4	3554	22485	22989
5	4864	31703	32206
6	3427	21829*	22331*
7	4693	29897*	30406*
8	4361	28265	28767
9	3681	23935	24428
10	1815	11929*	12215*

(B)

No. of image	No. of the calculated COG	ΣΔX	ΣΔY
1	3770	45857	45857
2	2821	38572	38572
3	3548	42215	42215
4	3554	41961	42466
5	4864	49251	49251
6	3427	51005	51005
7	4693	35685	35685
8	4361	44785	44785
9	3681	47527	47527
10	1815	20187	20187

(C)

No. of image	No. of the calculated COG	ΣΔX	ΣΔY
1	3770	45857	45857
2	2821	38572	38572
3	3548	42215	42215
4	3554	41961	42466
5	4864	49251	49251
6	3427	51005	51005
7	4693	35685	35685
8	4361	44785	44785
9	3681	47527	47527
10	1815	20187	20187

(D)

From Table 3, it could be noticed from the results in (A) and (B) that 50% of the summation errors of coordinates are different between the 1st iteration and the 2nd iteration of running *Algorithm-1*. The different results are highlighted and marked with star (*) symbol in (A) and (B). In parts (C) and (D) of Table 3, it could be noticed that the results are constant and there is no single difference between the 1st and the 2nd iterations. Therefore, this can prove that the new equations can always give the exact location of CoGs which is supposed to be located at the center of vessels no matter how many the program (*Algorithm-2*) runs. This is because the new equations depend on the gray scale value of the vessels. To confirm this fact, both algorithms are run on the same 10 angiograms of Table 3 but with T= 21. Once more, there was 50% difference in the results of *Algorithm-1* ((A) and (B)) while there was none in the results of *Algorithm-2* ((C) and (D)). Table 4 shows the results of applying both algorithms with T = 21 and on the same 10 angiograms.

TABLE IV
T = 21. FIRST ITERATION OF RUNNING *ALGORITHM-1* ON 10 ANGIOGRAMS. B) SECOND ITERATION OF RUNNING *ALGORITHM-1* ON THE SAME 10 ANGIOGRAMS. C) FIRST ITERATION OF RUNNING *ALGORITHM-2* ON THE SAME 10 ANGIOGRAMS. D) SECOND ITERATION OF RUNNING *ALGORITHM-2* ON THE SAME 10 ANGIOGRAMS.

No. of image	No. of the calculated COG	$\sum \Delta X$	$\sum \Delta Y$
1	6076	26365	26869
2	5466	23343*	23371*
3	6906	29522	30026
4	6963	28705	29210
5	9142	39601	40104
6	7051	28129*	28170*
7	9531	38569	39078
8	8805	36390*	36418*
9	6752	29278*	29500*
10	3038	13982*	14099*

(A)

No. of image	No. of the calculated COG	$\sum \Delta X$	$\sum \Delta Y$
1	6076	26365	26869
2	5466	23648*	24154*
3	6906	29522	30026
4	6963	28705	29210
5	9142	39601	40104
6	7051	28303	28805
7	9531	38569	39078
8	8805	36655*	37157*
9	6752	29559*	30052*
10	3038	14281*	14567*

(B)

No. of image	No. of the calculated COG	$\sum \Delta X$	$\sum \Delta Y$
1	6076	58395	58395
2	5466	46856	46856
3	6906	53712	53712
4	6963	55027	55532
5	9142	65765	65765
6	7051	62771	62771
7	9531	45329	45329
8	8805	55111	55111
9	6752	58347	58347
10	3038	22985	22985

(C)

No. of image	No. of the calculated COG	$\sum \Delta X$	$\sum \Delta Y$
1	6076	58395	58395
2	5466	46856	46856
3	6906	53712	53712
4	6963	55027	55532
5	9142	65765	65765
6	7051	62771	62771
7	9531	45329	45329
8	8805	55111	55111
9	6752	58347	58347
10	3038	22985	22985

(D)

We depended on three assumptions in this paper to prove the correctness and robustness of the new proposed equations over the conventional equations to calculate the CoG points. As it was mentioned earlier in this paper, the conventional equations involve the coordinate values of images only for CoG calculation. However, our new equations involve, beside the coordinates, the gray scale value of pixels. The new equations work on the masked angiograms to calculate the centroids of arteries. The three assumptions that were used in this paper and their observations are summarized in Table 5.

TABLE V
THE THREE ASSUMPTIONS AND OBSERVATIONS OF THE NEW PROPOSED COG EQUATIONS OVER THE CONVENTIONAL.

Conventional equations	Proposed equations
In the normal cases $\sum \Delta X \neq \sum \Delta Y$	In the normal cases always $\sum \Delta X = \sum \Delta Y$
Running the program more than once sometimes produces $\sum \Delta X \neq \sum \Delta Y$	Running the program more than once always produces $\sum \Delta X = \sum \Delta Y$
False results will appear because the equations depend only on the x and y axes in the calculation of the CoG	False results will not appear because the equations depend on the x and y axes plus the intensity value in the calculation of the CoG

The first observation of getting different results locations from *Algorithm-1* but not from *Algorithm-2* is occurred because the new equations can calculate CoG points exactly in the centers of vessels but this is not the case with the conventional equations. The second observation getting different results with *Algorithm-1* but always the same results with *Algorithm-2* when both algorithms run multi times is occurred because the conventional equations follow the coordinates of the arteries only but the new equations follow the coordinates and the gray scale of vessels. Therefore, the results with the conventional equations change in about 50% of angiograms but the results with the proposed equations are always fixed. The third observation of false alarms occurring with *Algorithm-1* but not with *Algorithm-2* is because the new equations follow and track the gray vessels until their end then stop calculating CoGs. However, the conventional equations keep calculating CoGs until the end of images and get errors linking the CoGs of end of the image with CoGs of the beginning.

IV. CONCLUSION

In this paper we presented a new approach to extract the coronary artery trees centerlines. This new approach used the technique of Center of Gravity with new proposed equations to extract CoG points. The algorithm starts by masking the plain angiogram images to highlight the coronary arteries only. Next, the masked angiogram is divided recursively using Recursion Data Structure technique. Next, with each division process and for each partition, find the number of points (gray pixels) per that partition or subpart (NoP). If $NoP \geq T$ (T is a threshold value), the partition or subpart is recursively divided again or else pass it to next step. Next, calculate a CoG point in the partition or subpart that failed the $NoP \geq T$ condition. The calculations of CoG points were done in this paper using both conventional and the proposed equations to compare the results and show the correctness and robustness of the proposed equations. The last step, after done calculating CoG points for the complete angiogram, is to link (connect) those centroids by lines to display the centerlines of the coronary artery trees as one shape. The results of comparing the proposed equations with the conventional proved that the new proposed equations can give more accurate results. The proposed approach in this paper is about extracting the centerlines of vessels in angiograms. This approach can be used in increasing the knowledge about the pixels of coronary arteries and their neighbors. The approach can detect exactly the neighbors of each pixel. This approach can be used in future work of detecting the locations of vessels in the coronary artery tree for medical benefits. We can conclude that the approach is a good tool to extract the centerline of the vessels and to help researchers get to know

and study the coronary artery trees in better shape. We hope to develop the approach in the future to show the connected lines of CoG points in three dimension shape.

ACKNOWLEDGEMENT

The authors of this paper would like to express their sincere thanks and appreciation to PPUKM hospital in Malaysia and the staff of angiograms imaging department for their cooperation in getting the data.

REFERENCES

- [1] J. E. Arlot, The determination of the center of gravity of a planet from photographic plates. *Celestial Mechanics and Dynamical Astronomy*. 26, 199-205 (1982).
- [2] S. P. Armes. The Center of Confusion: Otherwise Known as the Center of Gravity. 2006. Storming Media. Unclassified paper submitted to the Faculty of the Naval War College in partial satisfaction of the requirements of the Joint Military Operations Department.
- [3] S. R. Aylward and E. Bullitt, Initialization, noise, singularities, and scale in height ridge traversal for tubular object centerline extraction. *IEEE Trans. on Medical Imaging*. 21, 61-75 (2002).
- [4] D. S. Baim, *Grossman's cardiac catheterization, angiography, and intervention*. (Lippincott Williams & Wilkins Philadelphia: Baltimore, MD, 2000), pp. 558-558.
- [5] Edward D.Lemaire, Mario Lamontagne, Hugh W.Barclay, Thomas John and M. Guy Martel, A technique for the determination of center of gravity and rolling resistance for tilt-seat wheelchairs. *J. of Rehabilitation Research and Developmen*. 28, 51-58 (1991).
- [6] H. Goldstein, C. Poole, J. Saffo and S. R. Addison, *Classical mechanics*. *American J. of Physics*. 70, 782 (2002).
- [7] L. Guerra, M. Potkonjak and J. Rabaey, Divide-and-conquer techniques for global throughput optimization. In *IEEE Workshop on VLSI Signal Processing*, Citeseer, Berkeley, CA, USA, 1996, pp. 137-146.
- [8] Jonathan Thorne, M, e, T, Viren, A, nymous, luniu, lizzerand, Glutted and Goldenzebra, How to Calculate Center of Gravity, 2009. Retrieved 04 January 2011 from <http://www.wikihow.com/Calculate-Center-of-Gravity>
- [9] H. H. Khalil, R. O. K. Rahmat and W. A. Mahmoud, Estimation of Noise in Gray-Scale and Colored Images Using Median Absolute Deviation (MAD). In *IEEE 3rd International Conference on Geometric Modeling & Imaging*, London, UK, 2008, pp. 92-97.
- [10] H. H. Khalil, R. O. K. Rahmat, D. M. Zamrin, R. Mahmod and N. Mustapha, Three Dimension Reconstruction of Coronary Artery Tree Using Single-View Cineangiogram. *J. of Computer Science*. 6, 1485-1489 (2010).
- [11] H. H. Khalil, R. O. K. Rahmat, D. M. Zamrin, R. Mahmod and N. Mustapha, Three-Dimension Coronary Artery Tree Curvature Confirmation. *J. of Computer Science*. 6, 1524-1530 (2010).
- [12] A. Kitaoka, I. Kuriki and H. Ashida, The center-of-gravity model of chromostereopsis. *Ritsumeikan J. of Human Sciences*. 11, 59-64 (2006).
- [13] T. Luft, C. Colditz and O. Deussen, Image enhancement by unsharp masking the depth buffer. *ACM Trans. on Graphics (TOG)*. 25, 1206-1213 (2006).
- [14] K. Mori, S. Ema, T. Kitasaka, Y. Mekada, I. Ide, H. Murase, Y. Suenaga, H. Takabatake, M. Mori and H. Natori, A method for automated nomenclature of bronchial branches extracted from CT images. In *International Congress Series*, Elsevier, Nagoya, Japan, 2005, pp. 1281, 86-91.

- [15] A. Patwardhan, Subpixel position measurement using 1D, 2D and 3D centroid algorithms with emphasis on applications in confocal microscopy. *J. of Microscopy*. 186, 246-257 (1997).
- [16] S. Poteet, J. Patel, C. Giammanco, I. Whiteley, P. Xue and A. Kao, Words Are Mightier Than Swords and Yet Miscommunication Costs Lives. In *Proceedings of the Annual Conference of ITA (ACITA)*, London, UK, 2008.
- [17] M. R. Prince, T. M. Grist and J. F. Debatin, *3D contrast MR angiography*. (Springer Verlag, 2003).
- [18] Y. Sato, S. Nakajima, N. Shiraga, H. Atsumi, S. Yoshida, T. Koller, G. Gerig and R. Kikinis, Three-dimensional multi-scale line filter for segmentation and visualization of curvilinear structures in medical images. *Medical Image Analysis*. 2, 143-168 (1998).
- [19] H. C. Van Assen, M. Egmont-Petersen and J. H. C. Reiber, Accurate object localization in gray level images using the center of gravity measure: accuracy versus precision. *IEEE trans. on image processing*. 11, 1379-1384 (2002).
- [20] D. Vandermeulen, P. Plets, S. Ramkers, P. Suetens and G. Marchal. Integrated visualization of brain anatomy and cerebral blood vessels. In *Proceedings of the 1992 workshop on Volume visualization (VolVis92)*, ACM, NY, USA, 1992, pp. 39-46.
- [21] T. Zhang, H. B. Sipma and Z. Manna, Decision procedures for recursive data structures with integer constraints. *LECTURE NOTES IN COMPUTER SCIENCE*. 152-167 (2004).

Norwati Mustapha received her Diploma and B.Sc. in Computer Science; Universiti Pertanian Malaysia in 1988 and 1991 respectively. She received her M.Sc. (Information Systems); University of Leeds, UK in 1995 and her Ph.D. (Artificial Intelligence); Universiti Putra Malaysia, Malaysia. She is an Associate Professor at the Faculty of Computer Science and Information Technology, and head of computer science department. Her research interests are Intelligent Computing and Data Mining.

Hasan H. Khaleel was born in Iraq 1979. He received his B.Sc. in Electrical Engineering and M.Sc. in Control and Computer Engineering from University of Baghdad, in 2001 and 2003 respectively. He received his PhD in Computer Graphics from the faculty of Computer Science and Information Technology at University Putra Malaysia in 2012. Among his research interests and focus are Image processing, Computer Graphics, and Computer Assisted Surgery.

Rahmita O.K. Rahmat received the B.Sc. and M.Sc. degrees in Science Mathematics from University Science Malaysia, in 1989 and 1994, respectively. During 1989 to 1990 she work as research assistance in Department of Physics in University Science Malaysia experimenting on Ozone layer measurement at the Equatorial region, before working as tutor in Universiti Putra Malaysia. She received her PhD in Computer Assisted Engineering from University of Leeds, U.K. At this moment she is an Associate Professor working in Faculty of Computer Science and Information Technology as lecturer and acting as head of multimedia department. Among her focus research area are Computer Graphics and Applications, Computer Assisted Surgery and Computational Geometry.

DM Zamrin is a Professor and Consultant Cardiothoracic Surgeon at UKM Medical Centre, Kuala Lumpur, Malaysia (2006). He received his MD from the Universiti Kebangsaan Malaysia (1992) and post-graduate degree in Surgery (MMED Surgery) from Universiti Sains Malaysia (2000). He had his subspecialty training in cardiothoracic surgery at National Heart Institute (IJN), Kuala Lumpur, Malaysia (2000- 2003) and at Cardiothoracic Centre, Sarawak Heart Centre, Sarawak (2003 – 2004). He has performed more than 1,500 cardiac surgeries including coronary artery bypass grafts (CABG), aortic and mitral valve procedures, thoracic surgeries including lung resection for malignancies, video-assisted thoracoscopic surgery, endoscopic radial artery harvesting and endoscopic saphenous vein harvesting.

Ramlan Mahmud holds a PhD from University of Bradford, United Kingdom. He is currently a Professor at Faculty of Computer Science and Information Technology, Putra University of Malaysia and acting as the dean of the same faculty. His research area is artificial intelligence and security computing.